89

INTERFACIAL PROCESSES INVOLVING STRONG ELECTRONIC INTERACTIONS IN SOLAR ENERGY CONVERSION AND STORAGE*

HELMUT TRIBUTSCH

Hahn-Meitner-Institut für Kernforschung Berlin, Bereich Strahlenchemie, D-1000 Berlin 39 (F.R.G.)

Summary

It has been known for a long time that strong chemical bonding of intermediate species is necessary for efficient electrocatalysis, particularly of electron transfer mechanisms. This important aspect has been neglected in previous investigations of materials for fuel-producing and energy-storing photoelectrochemical reactions.

In order to emphasize this statement the progress of experiments with two groups of photoelectrodes which undergo strong interaction with reactants in the electrolyte is discussed. The first group consists of d band semiconductors (*e.g.* PtS_2 and RuS_2) in which the photogeneration of holes in the valence band derived from transition metal d states leads to the formation of interfacial coordination complexes with electron donors (*e.g.* OH^-). The second group consists of electrodes exhibiting combined electronic and ionic conduction which are able to photo-intercalate guest species (*e.g.* Cu^+ into $Cu_{6-x}PS_5I$ or Cu_3PS_4).

The behaviour of anodically polarized RuS_2 ($\Delta E_G = 1.2$ eV) as a stable photoelectrode which is able to liberate oxygen from water with a high quantum efficiency during illumination with visible and near-IR light confirms that complicated energy conversion reactions can take place in the presence of strong interactions even with thermodynamically unstable materials.

By comparing the performances of various ruthenium dichalcogenides it is shown that the photoelectrochemical reaction path depends strongly on the d state density in the upper region of the valence band. Energy losses due to kinetic inhibition (unfavourable energetic position of the intermediate states) can be reduced by using semiconductors containing transition metal pairs or clusters in their crystal structure.

Semiconductor materials which are able to photo-intercalate or photo-insert cations as a result of strong electron transfer interactions could be developed for light-powered ion pumps, intercalation batteries which can be charged by solar energy and systems capable of storing optical information.

Photoelectrode systems which undergo strong interactions with redox systems open up new perspectives for photoelectrochemical energy conversion and storage but also demand major research efforts. New materials with specific electronic and interfacial properties for which simplified electron transfer models are not adequate need to be developed. It will also be necessary to deal with high concentrations of surface states.

1. Introduction

Since the photoelectrolysis of water was proposed as a feasible mechanism for energy conversion and storage approximately 15 years ago [1], many efforts have been made to improve its efficiency and spectral sensitivity. In addition to TiO_2 [1] many other oxides [2 - 7] as well as commercial semiconductors coated with thin metal layers [8 - 12] have been tested as materials for photoelectrolysis. Scientific understanding of photoelectrochemical reactions which convert energy and produce fuel has rapidly increased [13] and a number of interesting proposals have emerged in recent years. However, a high performance electrode material for the solar photoelectrolysis of water has not yet been developed. TiO_2, which was the first semiconducting compound suggested for this purpose, still appears to have the best performance although its solar energy conversion efficiency is only a modest 0.7%. The theoretical optimum efficiency of photoelectrolysis using only one semiconductor has been estimated to be 12%. A solar cell utilizing the combined action of a photovoltaic and a photoelectrochemical semiconductor junction (tandem configuration) could reach an efficiency of 23% [13]. Comparable values have recently been calculated by Weber and Dignam [14] for solid—electrolyte junctions with high fill factors (11.6% and 22% respectively). The optimum efficiency for p—n photoelectrochemical cells has been estimated to be 16.6%.

Although efficient single-photon photoelectrochemical junctions with an energy gap ΔE_G of 2.2 eV in which electron and hole quasi-Fermi levels can reach the electrochemical redox energy levels of the $H^+|H_2$ and $O_2|H_2O$ couples are feasible, two-photon systems (the p—n photoelectrochemical cell and the tandem photoelectrochemical cell) promise much higher efficiencies. In this case, however, photoanodes with energy gaps of less than 2.2 eV will be needed.
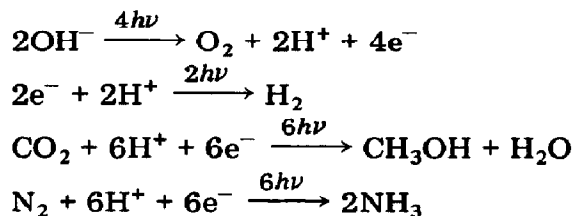
Experience shows that semiconductor electrodes with low energy gaps tend to be thermodynamically unstable. If electrodes of this type are developed for photoelectrolysis, photocorrosion must be kinetically inhibited. This requires careful energetic control of many-electron transfer reactions such as oxygen evolution from water which must proceed at a lower electrode potential than the corrosion reaction.

2. Strong interaction in electrocatalysis

The development of photoelectrodes which are capable of strong interactions with redox systems in the electrolyte has been neglected in the past. In contrast, electrodes which generate low concentrations of surface states and undergo electron transfer by tunnelling processes with negligible interactions have been preferred. Metal oxides with large energy gaps (*e.g.* TiO_2 and $SrTiO_3$), semiconductor electrodes characterized by low concentrations of surface states and electron exchange by tunnelling mechanisms (*e.g.* CdS), and photoactive materials containing elements which tend not to form suitable chemical complexes (*e.g.* GaAs, InP and silicon) do not provide favourable conditions for strong reversible interactions. Both the electronic and the photoelectrochemical properties of semiconductor electrodes must be tailored for strong selective interactions.

The role of strong interactions between an electrode and the redox components has already been discussed with respect to the catalysis of electrochemical dark reactions [15]. Strong interactions are particularly advantageous for multistep redox reactions in which intermediates with high activation energies must be generated before the reaction can proceed to the final product. Owing to the strong interaction of these intermediates with the electrode the reaction rate can, as is known from all practical examples of efficient electrocatalysis, increase in a sensitive way.

All the main photoelectrochemical reactions which are of interest for the production of fuel using solar energy belong to this class of reaction, *e.g.*

$$2OH^- \xrightarrow{4h\nu} O_2 + 2H^+ + 4e^-$$

$$2e^- + 2H^+ \xrightarrow{2h\nu} H_2$$

$$CO_2 + 6H^+ + 6e^- \xrightarrow{6h\nu} CH_3OH + H_2O$$

$$N_2 + 6H^+ + 6e^- \xrightarrow{6h\nu} 2NH_3$$

The consequences of strong interactions of the intermediates of such energy conversion reactions are far reaching (Fig. 1). The reactants enter the Helmholtz double layer and electrostatic forces become important for all redox species with an excess electric charge or dipole moment. The structure of the double layer can thereby undergo marked changes. The outer solvation shell, and in many cases the inner solvation shell also, is reorganized. Some ligands may also be lost as compensation for the strong interactions with the electrode. The distance from the surface for electron transfer becomes more important as the interaction energy becomes stronger. A multidimensional representation of energy surfaces for describing electron transfer and calculating activation energies becomes unavoidable. Under favourable conditions the rate of electron exchange with strongly adsorbed species may become so high that different oxidation states become indistinguishable [16]. In the limiting case of very strong interaction the electron exchange levels of the adsorbed species can be treated as surface states of the
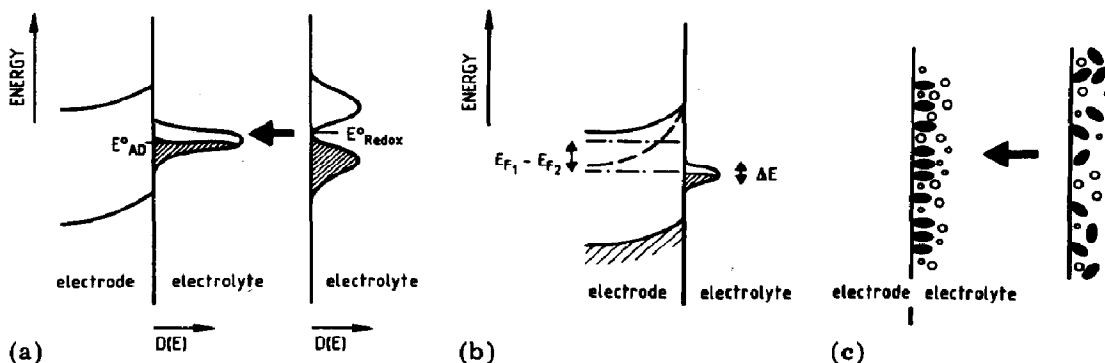
Fig. 1. Examples of the effects exerted on electrode interfaces by strong molecular interactions: (a) the electron exchange energy levels of redox couples become surface states; (b) the electrode potential affects the energetic position of redox surface states; (c) the Helmholtz layer is restructured.

electrode. When the donor state has an electric charge (*e.g.* OH^-) its energy in the adsorbed state will depend on the local potential in the double layer. This will also be true for the acceptor state (*e.g.* $OH_{ad} + e^-$). It is clear from these considerations that the distribution of the electron exchange energy levels of redox couples which interact strongly with electrodes will deviate substantially from that calculated for solutions. The electronic states of the redox couples almost become part of the electronic system of the electrode, and their degree of occupation becomes dependent on the position of the Fermi level in the electrode.

It can be shown that the highest rates and most efficient catalysis are expected when the redox energies of all the individual electron transfer steps in multielectron transfer reactions are almost the same. This will only occur when the intermediates bond strongly with the electrode surface and their electronic levels couple with the electronic system of the electrode.

3. Materials capable of strong photo-induced interfacial interactions

For efficient photoelectrocatalysis it is not sufficient to select semiconductor electrodes according to the width of the forbidden energy gap and the position of the flat-band potential. In addition, it appears to be necessary to tailor the electronic, chemical and crystalline properties of semiconducting materials in such a way that a specific chemical interaction can be induced during illumination. This is not a simple task and much more experience will be needed before generalized rules can be derived for more systematic approaches. In this paper we shall limit ourselves to two classes of examples which we have investigated in some detail (Fig. 2).

The first concerns the attempt to generate, through illumination, an interfacial coordination complex which binds electron-donating species. In order to facilitate the uptake of an electron-donating ligand into the
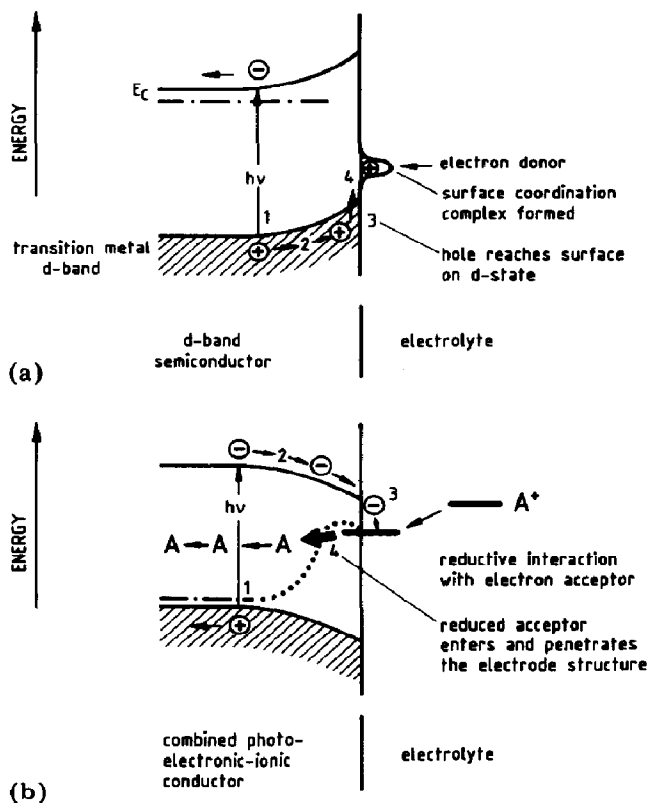
Fig. 2. Two different classes of photoelectrode in which strong interfacial reactions are facilitated: (a) d band semiconductors which form surface coordination complexes; (b) host materials for light-induced intercalation or insertion of ions.

coordination shell of a surface transition metal, which is a constituent of the electrode, photogenerated holes have to undergo electrochemical reactions from the transition metal d states (Fig. 2(a), reaction sequence 1 - 4). Only the arrival of a positive hole at a transition metal d state can increase the transition metal oxidation state, thus inducing completion of coordination. The search for semiconducting materials which derive their valence band from transition metal d states started in 1977 with MoS_2 [17, 18], continued with $MoSe_2$, WS_2 and WSe_2 [19 - 28] and at present includes materials such as PtS_2 [29], RuS_2 [29 - 33], FeS_2 [34 - 36], ReS_2 [37] and RuP_3 [38].

All the d band semiconductors investigated so far photoreact with water (Table 1) and demonstrate unusual electrocatalytic properties in many-electron transfer reactions. These properties were found to be independent of the crystal structure, which was layer type (MoS_2, WS_2 and PtS_2), pyrite type (RuS_2 and FeS_2) or triclinic with space group $P\bar{1}$ (number 2 in ref. 40). The fact that the electrodes photoreact with water is strictly correlated with the d character of their valence bands and thus with the supply of holes to transition metals at the electrode surface (Fig. 3). ZrS_2,

TABLE 1

Properties of semiconductors with valence bands derived from transition metal d states and of the products of their photoelectro-chemical reactions with water

| Compound	T–T distance (Å)	Energy gap (eV)	O–O △ T	O=O ‖ T	Oxidation state of T	Crystal structure	Photoelectro-chemical products	Reference
MoS_2	3.2	1.13 - (1.6)	+		Medium	Layer type	SO_4^{2-}	[18]
WS_2	3.2	1.2 - (1.6)	+		Medium	Layer type	SO_4^{2-}	[23]
PtS_2	3.6	0.95	+		High	Layer type	O_2	[29]
RuS_2	3.9	1.2	+		High	Pyrite	O_2	[30 - 33]
FeS_2	3.8	0.95		+	Low	Pyrite	SO_4^{2-}	[34 - 36]
ReS_2	2.6 - 2.9	1.4	+		High	Layer type	O_2 ?, ReO_x	[39]
RuP_3	2.8	1.67	+		High	Triclinic $P\bar{1}$	PO_4^{3-}, RuO_4, O_2	[38]

T, transition metal
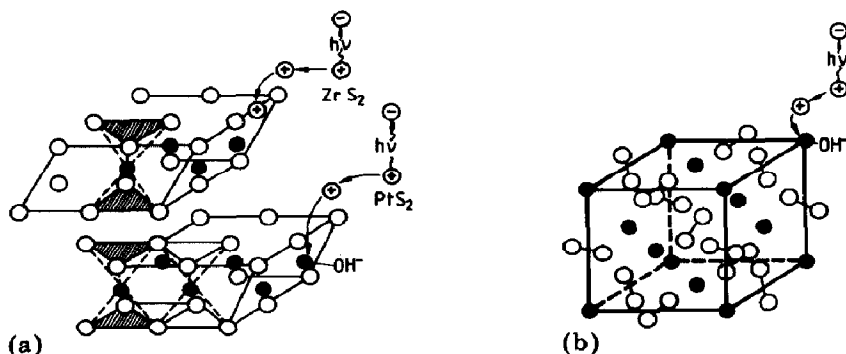
Fig. 3. Crystal structures (a) for PtS$_2$ and ZrS$_2$ (layer type) (○, S; ●, Pt, Zr) and (b) for RuS$_2$ and FeS$_2$ (pyrite type) (○, S; ●, Ru, Fe). The transfer route for photogenerated holes (reacting with transition metal atoms or breaking chemical bonds in the electrode surface) is shown.

which has a crystal structure identical with that of PtS$_2$ but a valence band derived from the sulphur p states, cannot supply holes to the transition metal and photocorrodes to molecular sulphur and zirconium ions [41].

The second group of materials which are able to undergo strong interfacial interactions during illumination are the combined electronic–ionic conductors which can take up, exchange or release guest atoms or molecules as a consequence of the variation of the electrochemical potential of the electrode. The change in the quasi-Fermi level for electrons or holes during photo-induced intercalation or deintercalation is the driving force for the transfer of the guest species across the electrode–electrolyte interface (Fig. 2(b)). Light-induced intercalation and insertion reactions were first described and discussed in 1980 [42, 43].

The range of compounds which can act as host materials comprises many crystal classes and chemical compositions. Many semiconducting materials with favourable energy gaps between 1 and 3 eV are included among them. Various aspects of these photo-induced ionic mechanisms have been discussed on the basis of experimental results obtained using host materials of the composition MX, MX$_2$, MPX$_3$, M$_3$PX$_4$, M$_{6-x}$PX$_5$Hal, MO$_2$ and (CH)$_n$ (M $\equiv$ metal; X $\equiv$ S, Se; Hal $\equiv$ halogen) [44] (Table 2). Layer-type transition metal dichalcogenides such as ZrSe$_2$ [42], HfSe$_2$ [45] and ZrS$_2$ [46] proved to be of limited interest for photo-intercalation reactions because intercalation of only a few per cent of cations produced degeneration and quasi-metallic behaviour of the host material with a consequent loss of the photoeffect. Host materials of composition MPS$_3$, e.g. FePS$_3$, had a photoeffect with a quantum efficiency which was too small. InSe in contact with propylene carbonate exhibited more favourable behaviour [47, 48], but the most promising results were obtained with the new perovskite-related modification TiO$_2$(B) [49] and with the semiconductors Cu$_3$PS$_4$ [50] and Cu$_{6-x}$PS$_5$I [51]. TiO$_2$(B) intercalates hydrogen from water without suffering irreversible corrosion damage like that observed with layer-type transition metal dichalcogenides. Cu$_{6-x}$PS$_5$I and related compounds

TABLE 2

Semiconducting materials used for photo-intercalation and photo-deintercalation experiments

Compound (host material)	Energy gap (eV)	Conduction type	Intercalated (guest) species	Electrolyte	Observed photoreaction	Reference
$ZrSe_2$	1.05 - 1.22	p	Li	Acetonitrile	Photo-intercalation	[42]
$HfSe_2$	1.13	n	Na	Acetonitrile	Photo-deintercalation	[45]
ZrS_2	1.68	n	Na	Acetonitrile	Photo-deintercalation	[46]
$FePS_3$	1.5	p	Li	Acetonitrile	Photo-intercalation	[44]
InSe	2	n, p	Cu	Propylene carbonate	Photo-(de)intercalation	[47, 48]
$TiO_2(B)$	3	n	H	Water	Photo-deintercalation	[49]
Cu_3PS_4	≈ 2	p	Cu	Acetonitrile	Photo-intercalation	[50]
$Cu_{6-x}PS_5I$	2.05	p	Cu, Ag	Acetonitrile	Photo-intercalation	[51]
$(CH)_n$	1.5	p	ClO_4	Acetonitrile	Photo-deintercalation	[52]

maintain good semiconducting properties despite the occurrence of substantial stoichiometric variations during photo-intercalation reactions. Interesting photo-intercalation properties are also encountered with semiconducting polymers of acetylene, thiophene and other molecular species. They are relatively easily produced, easy to alter chemically and can be intercalated (doped) by a large variety of guest molecules.

The presence of a strong interaction between an illuminated host electrode and a reacting guest species can easily be verified (Fig. 4). The reductive photo-intercalation of cations takes place at much more positive potentials than does pure photoreduction. The oxidative photo-intercalation of anions occurs at more negative potentials than does pure photo-oxidation of the anion. Thus electron transfer is also associated with a strong interfacial interaction in these cases.

The following examples serve to demonstrate the use of mechanisms involving strong interactions.
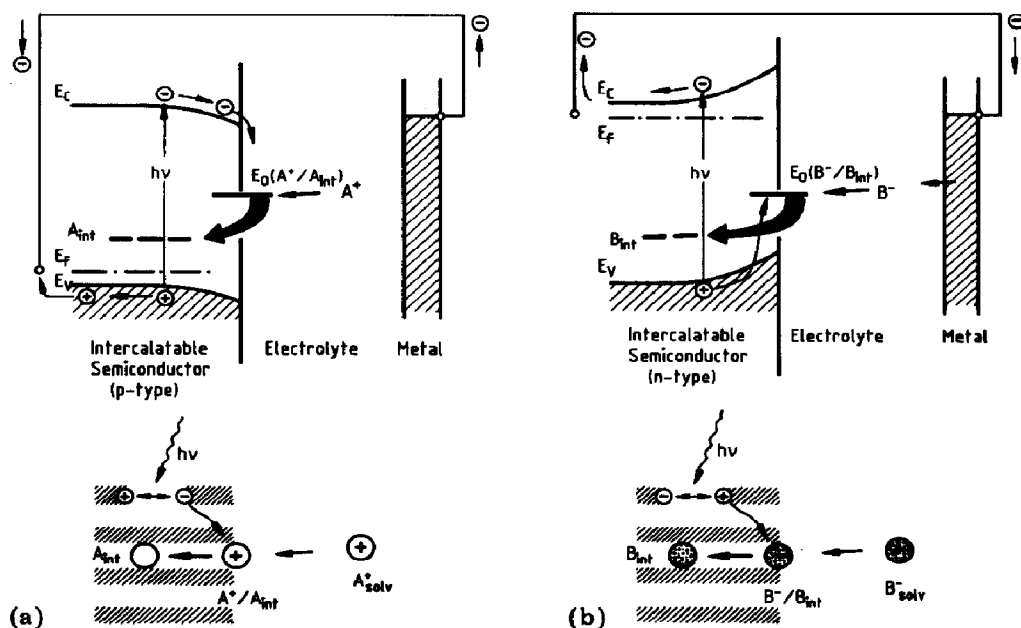

Fig. 4. Energy diagram (above) and schematic representation (below) of the light-induced intercalation of (a) cations and (b) anions.

4. Photoelectrolysis with RuS$_2$

Although all semiconducting d band sulphides investigated so far (Table 1) photoreact with water, it was found not to be a straightforward matter to channel the complete reaction into oxygen evolution. Semiconducting materials such as MoS$_2$, WS$_2$ and FeS$_2$ yielded the metal sulphate as the principal oxidation product. PtS$_2$ liberated oxygen from water under

illumination although the overpotential was high [29]. RuS_2 finally photoreacted with water in the presence of a moderate overpotential [30 - 33]. To understand this situation it has to be remembered that all these transition metal disulphides are thermodynamically unstable with respect to corrosion. Photo-induced oxygen evolution and stability against corrosion, as is found in the case of RuS_2, can only be understood as a consequence of kinetic stabilization. This is explained in Fig. 5. Holes arriving for reaction at electron d states, which do not represent bonding states, cannot induce corrosion as long as the activation energy $\Delta G^{\ddagger}$ for oxygen evolution is sufficiently small. As a consequence of the strong coordination-type bonding of the intermediates of the oxidation of water $\Delta G^{\ddagger}$ is less than the activation energy for photocorrosion to ruthenium sulphate. As has been shown elsewhere [39, 41], the contribution of the electric potential drop $e\Delta\varphi_{SE}$ in the Helmholtz layer must be taken into account in a more complete formula describing the kinetic requirements for the photo-oxidation of water.

The d band semiconductor RuS_2 which channels photogenerated holes into oxygen evolution via ruthenium-based coordination complexes was found to have a complicated solid state chemistry. Samples grown from liquid tellurium by slow sublimation of tellurium had an apparent energy gap ΔE_G of 1.85 eV [30]. A much faster growth technique in which the
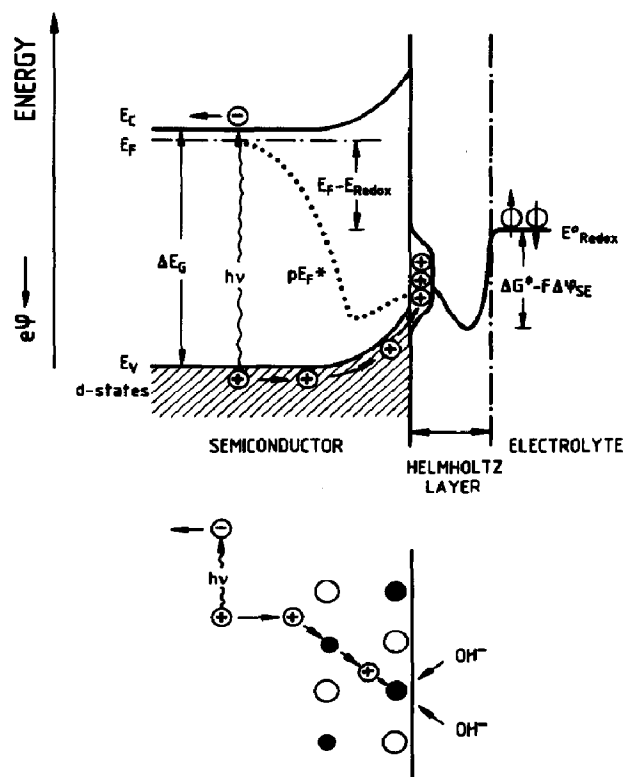

Fig. 5. Energetic and kinetic quantities accounting for the ability of a photoelectrode to photoreact with water: ●, transition metal; ○, sulphur.

tellurium in iron-containing RuS_2 crystals was removed using aqua regia also yielded samples with ΔE_G as low as 1.15 eV [31, 32]. The growth of RuS_2 from liquid bismuth yielded samples with $\Delta E_G = 1.2$ eV but with marked variations in the IR sensitivity [33, 53] (Fig. 6(a)). It is tentatively suggested that deviations from stoichiometry in the pyrite lattice (Fig. 3) could account for these variations. When sulphur atoms are absent from the coordination shell of ruthenium, the d states will shift into the otherwise forbidden energy region and decrease the apparent energy gap. Since the quantum efficiency for oxygen evolution with IR photons with $h\nu = 1.4$ eV achieved 23% we describe this material as IR-sensitive RuS_2 with an energy gap of 1.2 eV. This material is the most favourable at present since it is a more efficient collector of solar radiation than the IR-insensitive compound with comparable electrochemical properties. The IR sensitivity of FeS_2 with the same crystal structure as RuS_2 also showed variations but they were less pronounced (Fig. 6(b)).

The excellent photoelectrochemical properties of RuS_2 grown from liquid bismuth are shown in Fig. 7 for the liberation of oxygen from water. The complete photoelectrochemical reaction is channelled into the liberation of oxygen which can be detected at 1 V (measured with respect to a normal hydrogen electrode (NHE)), i.e. below the thermodynamic potential $E°$ of 1.23 V to which an overpotential of approximately 0.25 V would have to be added to reach comparable current densities. Perfect limiting current behaviour was observed where quantum efficiencies of up to 60% were measured with short wavelength visible light. Photocurrent densities for
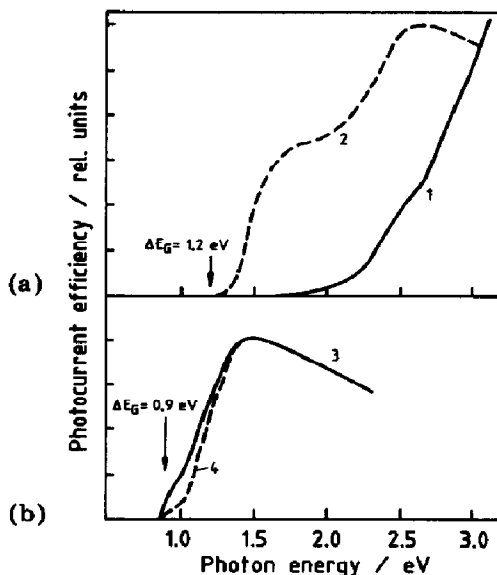

Fig. 6. Spectral dependence of the photocurrent efficiency (relative units) of (a) RuS_2 grown from bismuth (curve 1, IR insensitive; curve 2, IR sensitive) and (b) FeS_2 grown by vapour transport (curve 3, synthetic $FeS_2|I^-|I_2$ electrolyte; curve 4, natural $FeS_2|I^-|$ I_2 electrolyte).
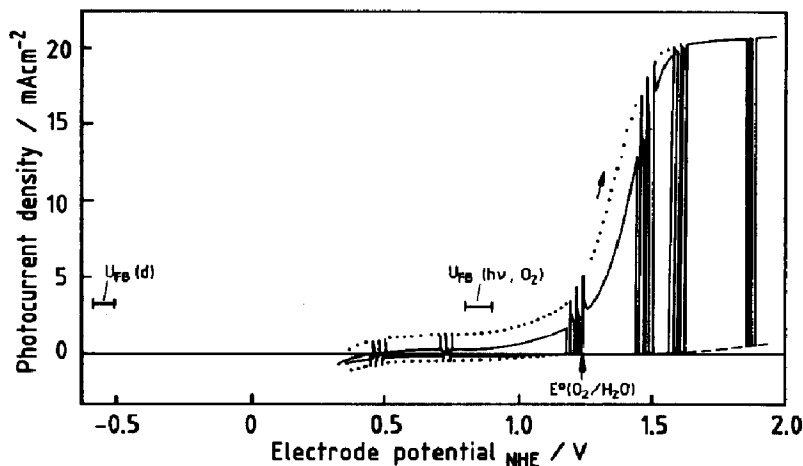
Fig. 7. Photocurrent density–voltage behaviour of oxygen-liberating RuS_2 in 1 N H_2SO_4. The flat-band potential $U_{FB}(d)$ in the dark and the flat-band potential $U_{FB}(h\nu, O_2)$ during oxygen evolution, which is extrapolated from measurements in the limiting photo-current region, are indicated.

oxygen evolution of up to 170 mA cm^{-2} were observed using concentrated light from a 250 W tungsten lamp. Figure 7 also shows a pronounced relaxation of photocurrents after interruption of illumination, which disappears in the saturation region. Apart from small traces of volatile RuO_4 detected at high electrode potentials ($U > 1.5$ V (NHE)) no indication of photocorrosion was found. Even after passage of 1000 C cm^{-2} no corrosion patterns were detected on the RuS_2 surface [32].

Figure 8 shows a semilogarithmic plot of the photocurrent densities measured with RuS_2. The photocurrent densities are plotted against the overpotential of the $O_2|H_2O$ redox couple. Although photocurrent density–voltage curves cannot be interpreted in terms of Tafel plots, a comparison is useful for energetic reasons. An oxygen evolution curve obtained with RuO_2 [54] is also shown in Fig. 8. The photoevolution of oxygen using RuS_2 with an energy gap ΔE_G of only 1.2 eV cannot proceed without a supporting electrode potential, but the energy gain is positive. The hypothetical curve displaced 0.4 V to the left will be discussed as the theoretical limit of RuS_2 provided that further favourable modifications can be made to the intermediate surface coordination complex (see later). Figure 8 also shows that photo-induced chlorine evolution is energetically more efficient than oxygen evolution although the redox potential of the $Cl^-|Cl_2$ couple is more positive ($E^\circ = 1.37$ V).

The energetic situation encountered for RuS_2 ($\Delta E_G = 1.2$ eV) during photo-induced electrolysis (assumed polarization, 1 - 1.2 V (NHE)) is shown in Fig. 9. It can be seen that the valence band of TiO_2, which is also shown in Fig. 9, is situated up to 1 eV below that of RuS_2. However, TiO_2 ($\Delta E_G = 3$ eV) needs a supporting voltage ΔV of only 0.2 V for the photoelectrolysis of water into oxygen and hydrogen. The RuS_2 system is clearly energetically more favourable. Moreover it can utilize low energy photons with high
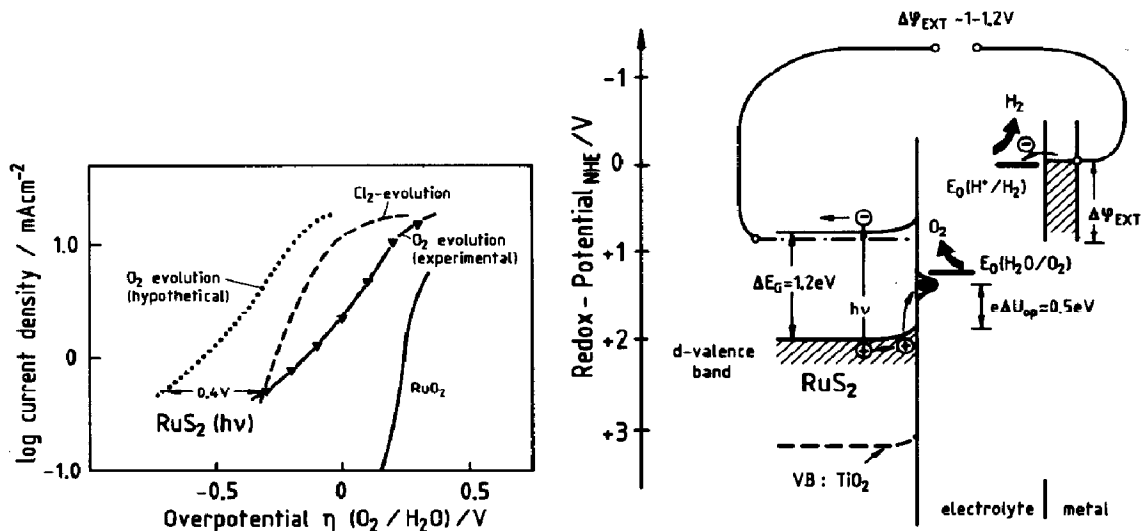
Fig. 8. Logarithmic plot of the photocurrent density due to oxygen evolution as a function of the overpotential $\eta(O_2|H_2O)$. The curve of photocurrent density due to chlorine evolution and the hypothetical oxygen evolution curve for an RuS_2 electrode without energy loss due to kinetic inhibition ($\Delta V \approx 0.4$ V) are included for comparison.

Fig. 9. Positions of the energy bands of RuS_2 ($\Delta E_G = 1.2$ eV) in a photoelectrolysis cell during potential-assisted electrolysis. The position of the valence band edge of TiO_2 during photoelectrolysis is shown for comparison.

quantum efficiency. In Fig. 9 we have indicated surface states 0.5 eV above the edge of the valence band which should serve as intermediate states for hole transfer to the $O_2|H_2O$ redox couple. Their position was estimated in the following way. As mentioned before, capacity measurements performed during the liberation of oxygen by RuS_2, which are technically possible owing to the constant limiting current of the electrode, yielded a flat-band potential $U_{FB}(h\nu, O_2)$ of 0.8 - 0.9 V (NHE) [33] which is strongly shifted in the positive direction. This result justifies the energy band position of RuS_2 shown in Fig. 9. Further supporting evidence is that oxygen evolution is detectable at a cell voltage of 1 V (NHE) (qualitative confirmation is obtained by gas chromatography). Figure 10 shows how the energy bands of RuS_2 shift from their position at equilibrium (left-hand side) to their position during oxygen evolution (right-hand side). It can easily be seen from this figure, in which the energetic situation with IR-sensitive RuS_2 ($\Delta E_G = 1.2$ eV) is compared with that encountered in IR-insensitive RuS_2 ($\Delta E_G \approx 1.85$ V), that the RuS_2 samples with low energy gaps (see Fig. 6(a)) exhibit more favourable behaviour. Much less energy (0.5 eV compared with 1.15 eV) is lost as a result of the relaxation of holes into the surface state which serves as an intermediate level for hole transfer. To estimate the energetic position of these intermediate states in IR-sensitive RuS_2 it must be remembered that the onset of photocurrent shifts in a systematic way as the redox systems are changed (Fig. 11). A plot of the electrode
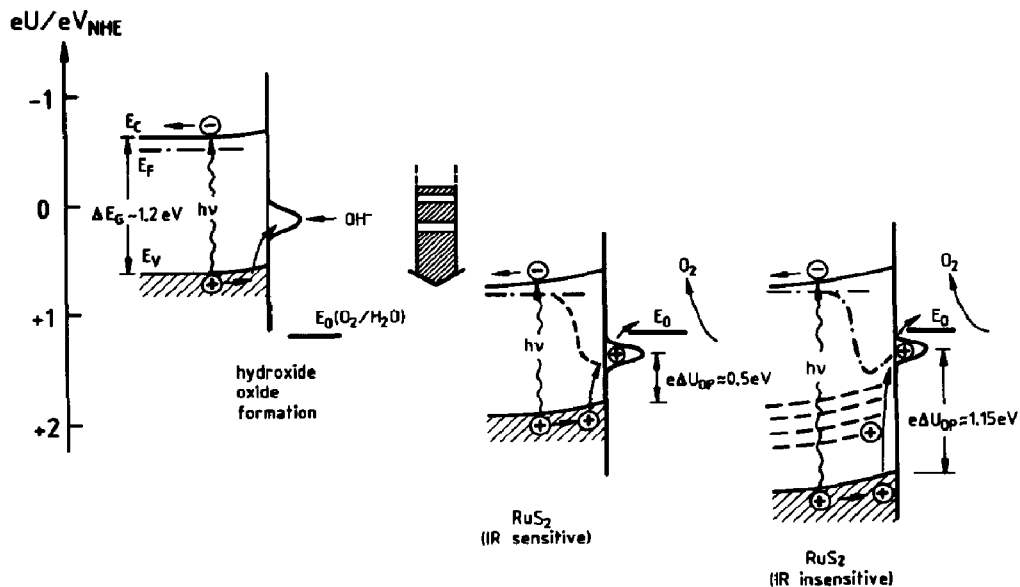
Fig. 10. Positive shift of the energy bands of RuS_2 from the dark position to the situation during the photoevolution of oxygen. The energetically less favourable situation with an IR-insensitive RuS_2 sample is also shown.
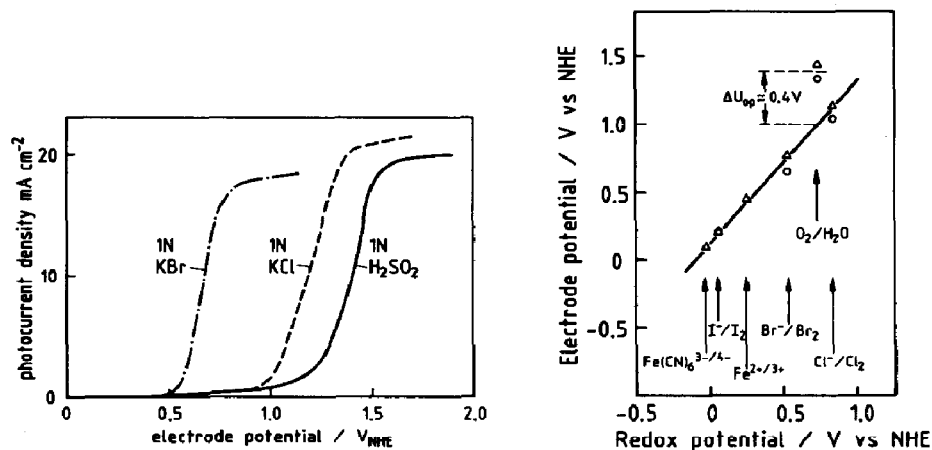

Fig. 11. Shift of the photocurrent density—voltage curves as the redox system is changed.

Fig. 12. Electrode potentials at which a constant photocurrent density (10 mA cm^{-2}) is reached in the presence of various redox systems. Results obtained with RuS_2 grown from tellurium ($\triangle$) and bismuth ($\bigcirc$) are compared.

potentials at which a given photocurrent density (10 mA cm^{-2}) is reached as a function of the redox potential of the electrolyte yields a straight line (Fig. 12) which indicates that the valence band of the RuS_2 electrode adjusts itself to the energy levels of the redox couples. Only the $O_2|H_2O$ couple does not fit into this scheme. An additional electrode potential ΔU_{OP} of about

0.4 V has to be applied to initiate photo-induced hole transfer. The following estimate can now be made. From capacity measurements it can be deduced that during oxygen evolution the valence band is situated 0.7 V below the redox potential of the $O_2|H_2O$ couple. Since 0.2 V must be considered as an overpotential loss even with the best RuO_2-based electrodes, holes have to be transferred from surface states 0.2 eV below $E°(O_2|H_2O)$. They are thus situated $e\Delta U_{OP} = 0.5$ eV above the valence band (Fig. 9). The surface states responsible for hole transfer during one-electron transfer reactions are thus situated 0.4 eV deeper (Fig. 12) or 0.1 eV above the valence band, which is a reasonable conclusion.

Therefore the many-electron transfer process of oxygen evolution consumes an additional 0.4 eV compared with the one-electron mechanism owing to the formation of an unfavourable intermediate complex. Since metallic RuO_2-based oxygen-liberating electrodes do not produce such losses they must be considered specifically for the semiconducting disulphides used. The consumption of the additional 0.4 eV could, in principle, be avoided if the intermediate state responsible could be suitably modified and transformed. The potential difference $\Delta U_{OP} = 0.4$ V is therefore a measure of the improvement possible. We have included a hypothetical oxygen evolution curve for RuS_2 without the unfavourable transition complex in Fig. 8. It can be seen that, at a photocurrent density of 10 mA cm^{-2}, illuminated RuS_2 ($\Delta E_G = 1.2$ eV) requires a cell voltage 0.6 V less than that required by RuO_2 in the dark. This corresponds to 50% of the semiconductor energy gap. The semiconductor would therefore approach the thermodynamic limitations for photoelectrolysis.

The successful synthesis of the semiconducting ruthenium dichalcogenides RuS_2, $RuSe_2$ and $RuTe_2$ with identical pyrite structures facilitated further testing of the d band concept for the photoelectrocatalysis of many-electron transfer reactions like the electrolysis of water [55]. The thermodynamic decomposition potential of these ruthenium dichalcogenides only slightly varies on going from the sulphide to the telluride. The electrode stability should therefore not decrease on going from the sulphide to the telluride. However, experimental results contradict this thermodynamic prediction: with an RuS_2 electrode only oxygen is liberated and almost no corrosion occurs; with an $RuSe_2$ electrode with 80% of the holes oxygen is liberated and 20% accounts for a corrosion reaction; with an $RuTe_2$ electrode with 10% of the holes oxygen is liberated and the remainder (90%) accounts for a corrosion reaction. X-ray photoelectron spectroscopy (XPS) measurements of the valence band region of these compounds helped to resolve this apparent anomaly (Fig. 13). The ruthenium d states (t_{2g}) in RuS_2 are well separated from the lower-lying sulphur states so that the edge of the valence band consists only of d states. The chalcogen states approach the valence band edge in $RuSe_2$ and overlap the ruthenium states in $RuTe_2$. The contribution of tellurium states to the edge of the valence band of $RuTe_2$ thus explains the increased corrosion instability of this material. It should be emphasized that all three compounds are
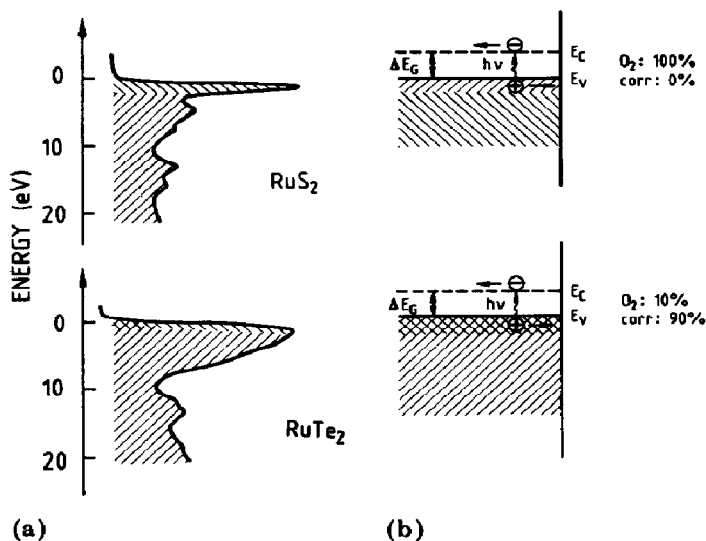
Fig. 13. (a) X-ray photoelectron spectra and (b) photoelectrochemical properties (energy band diagram) of RuS_2 and $RuTe_2$.

thermodynamically unstable and therefore should corrode. The stability of RuS_2 is only kinetic.

Thus as far as photoelectrolysis is concerned we have additional evidence for the need for d states as mediators for photo-induced many-step hole reactions. The surprisingly high overpotential loss ($\Delta U_0 = 0.4$ V) in the case of RuS_2 (Fig. 12) nevertheless indicates that some inhibition still occurs with this system. We have tried to understand this and have reached the following conclusion [39]. As can be seen in Table 1, the transition metal distances in MoS_2, WS_2, PtS_2, RuS_2 and FeS_2 exceed 3.2 Å and are thus too large for a cooperative reaction between two neighbouring metals in the electrode surface. The consequence is that the four-electron transfer reaction involving the oxidation of two OH^- ions to molecular oxygen proceeds entirely at individual transition metal centres. This requires that the transition metals are able to reach high oxidation states and to form peroxo-type complexes with oxygen. Only PtS_2 and RuS_2, which actually photo-oxidize water to molecular oxygen, satisfy these conditions. FeS_2, for example, makes a d state contribution to the valence band comparable with that of RuS_2 but photocorrodes to iron sulphate. The inability of iron to reach a sufficiently high oxidation state to bind two oxygen atoms must be the reason for the reaction of oxygen with sulphur to form $SO_4{}^{2-}$ as the final product. XPS measurements indeed detect high concentrations of SO_x groups on FeS_2 and negligible concentrations on RuS_2 [34]. One or two monolayers of oxide are detected on anodically polarized RuS_2; this is unavoidable for oxygen-liberating electrodes which have to bind the oxygen before releasing it in molecular form.

The energetic upward shift ($eU_{OP} = 0.5$ eV) of the electronic levels in the transition complex (Fig. 9) occurs because electron delocalization is

limited, and its ionization energy changes drastically as a consequence of the transfer of positive electronic charge [39]. In order to avoid such energetic shifts, the delocalization of electrons in these complexes must be increased: the electronic states in large potential wells are closer together than those in small potential wells. In order to increase delocalization it is reasonable to change from individual transition metal atom reaction centres to pairs or clusters of transition metal atoms (Fig. 14). Suitable anion ligands facilitate delocalization. The most favourable ligand is sulphur since it can easily mediate the d–d interaction and only slightly changes its ionization energy as a consequence of charge transfer. Oxygen is clearly less effective, as is shown by the low mobilities and narrow d bands in oxides.

Transition metal clusters can act as pools for holes and electrons which interact with donors (*e.g.* OH^-) or acceptors (*e.g.* H^+) and bind them to neighbouring sites for cooperative electron transfer while maintaining reasonably stable energetic conditions [39]. It is probably this advantage in electron transfer kinetics which has led to the evolution of such cluster complexes in biological structures involved in electrochemical energy conversion. Examples are 4Fe-ferredoxin (four iron atoms), 2Fe-ferredoxin (two iron atoms), the FeMo cofactor of nitrogenase (one molybdenum atom and three iron atoms), the manganese centre of photosynthesis (two manganese atoms) and oxyhaemocyanin (two copper atoms).

Materials containing metal-bonded species have not yet been seriously considered for electrochemical applications although they are being developed in increasing numbers owing to their unusual chemical and physical properties [56 - 59]. Semiconducting compounds, which we have started to investigate, have been identified among these materials (Fig. 14) [39]. In a typical system electrons involved in metal–metal bonding are the most
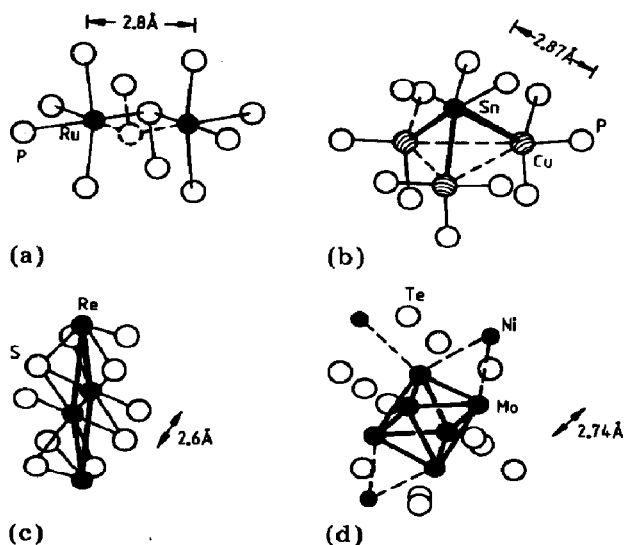

Fig. 14. Transition metal pairs or clusters (Ru_2, Cu_3, Re_4 and Mo_6) in semiconducting cluster compounds: (a) RuP_3; (b) Cu_4SnP_{10}; (c) ReS_2; (d) $Ni_{0.8}Mo_6Te_8$.

weakly bound and therefore occupy the edge of the semiconductor valence band. Transition metal cluster compounds with semiconducting properties are therefore promising candidates as d band semiconductors with improved kinetic behaviour. However, preliminary experiments have shown that the situation is complicated and that more experience is required before suitable new photoelectrodes can be unambiguously identified. For example, RuP_3 ($\Delta E_G = 1.67$ eV), which in the crystalline state possesses two ruthenium atoms separated by 2.8 Å, easily photoreacts with water but also generates PO_4^{3-} and RuO_4 species at a high rate [38]. Therefore it must be concluded that the phosphorus ligand is too easily oxidized and may not be suitable for photoelectrochemical applications. Cu_4SnP_{10} ($\Delta E_G = 1.1 - 1.2$ eV) also corrodes, and in this case XPS data indicate that the d states of copper do not form the edge of the valence band [60]. The Chevrel phases Mo_6X_8 ($X \equiv$ S, Se, Te) form an interesting class of transition metal cluster compounds. They are metallic conductors, but the partially empty conduction band can be filled by introducing transition metals with excess d electrons (e.g. $Mo_2Re_4S_8$ [61] or $Mo_4Ru_2S_8$ [62]). With $Ni_{0.8}Mo_6Te_8$ [63] (Fig. 14) we have found small photoeffects. ReS_2, which contains an Re_4 cluster with Re–Re distances as short as 2.6 Å, is a promising cluster compound for photoelectrolysis. Photoelectrochemical experiments have established an energy gap of 1.4 eV in this compound [39]. The X-ray photoelectron spectrum of ReS_2 clearly shows that rhenium d states form the top of the valence band (Fig. 15). According to our hypothesis this results in favourable conditions for photoelectrolysis, and in addition the transition metal is able to reach reasonably high oxidation states. n-type ReS_2 synthesized by vapour transport (ICl_3) yielded reasonably high photocurrent densities (Fig. 16) and photoreacted with water. Unfortunately, photodegradation gradually took place owing to oxidation of the material. It is possible that oxidized intermediate rhenium complexes are too stable for oxygen to be liberated. Nevertheless we believe that surface analytical techniques such as XPS and UV photoemission spectroscopy will prove to be very helpful in identifying d band semiconductors with transition metal clusters which are suitable photoelectrodes.
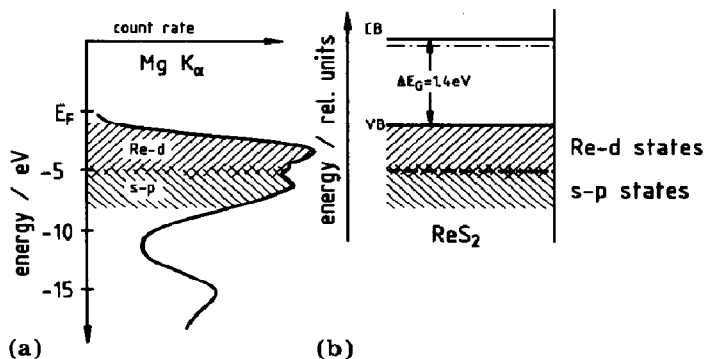

Fig. 15. (a) X-ray photoelectron spectrum of the valence band states and (b) qualitative energy scheme of the semiconducting Re_4 cluster compound ReS_2.
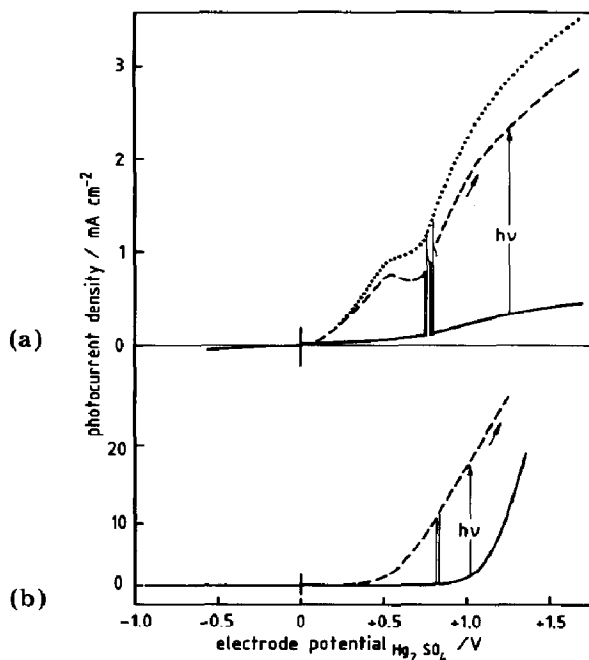
Fig. 16. Photocurrent density–voltage behaviour of (a) RuP$_3$ (ruthenium pairs) and (b) ReS$_2$ (R$_4$ clusters) (sweep, 10 mV s^{-1}; electrolyte, 1 N H$_2$SO$_4$).

5. The development of a cheap new solar energy material (FeS$_2$)

Our attention was attracted by FeS$_2$ (ΔE_G = 0.9 - 0.95 V) when we realized that it has the same crystal structure as and a similar electronic structure to RuS$_2$ [34]. As in the case of RuS$_2$, which we were able to develop for high photocurrent efficiencies, the top of the valence band of FeS$_2$ (pyrite) is derived from transition metal states. Therefore, like RuS$_2$, it reacts with water although sulphate and not oxygen is the main reaction product. Although natural FeS$_2$ was used as a semiconductor in early radio sets, nobody appears to have considered this material for solar applications. We have succeeded in developing electrochemical and photovoltaic solar cells using both synthetic single crystals [35] and polycrystalline material [36]. Quantum efficiencies of up to 92% have been observed, but so far photovoltages of only 0.27 V, which is much less than the theoretical maximum (0.5 V), have been obtained. The main difficulty with FeS$_2$, apart from the poor understanding of its crystal chemistry including doping, is the high concentration of surface states. As in the case of RuS$_2$ (Fig. 10) or other d band materials they cause the semiconductor energy bands to shift in the energy diagram. These surface states, which play a crucial role in current-producing solar cells, appear to be difficult to control by means of chemical etching with the standard agents used for the treatment of commercial semiconductors (e.g. acids and H$_2$O$_2$). Since the nature of these

states is not known and the X-ray photoelectron spectra provide little information (oxide and SO_x are detected) complementary research will be needed. Although solar energy conversion efficiencies for FeS_2 photoelectrochemical cells ($I^-|I_2$ electrolyte) do not exceed 1% at present, it is possible that this cheap material will be developed provided that the strong chemical interactions leading to the formation of surface complexes can be understood and adequately controlled.

6. Photo-induced ion transport

As a final example of interfacial energy conversion mechanisms involving strong interactions we shall discuss the promise of photo-intercalation reactions (Fig. 4) [44]. Complementary with the mechanisms described in Fig. 4 (photo-intercalation of cations in p-type semiconductors and anions in n-type semiconductors) the photo-deintercalation of cations from n-type materials and anions from p-type materials is also possible [44]. These mechanisms can be understood as light-driven topotactic redox reactions in which electrons and ions are simultaneously absorbed or released by the material surface. In an electrochemical cell, electrons are exchanged through the external circuit and ions are exchanged through the electrolyte. Since ions continuously cross the semiconductor–electrolyte interface as a consequence of the photogeneration of electron–hole pairs we can, in a simplified way, describe this phenomenon as "photo-induced ion pumping". This terminology is justified because ions are transferred against the chemical potential gradient in the dark. The driving force is evidently the photo-induced shift of the quasi-Fermi level for holes or electrons.

At first sight, photo-induced ion pumping might seem to be of limited interest, mainly because of the absence of information on photosensitive ion conductors. However, the list of materials investigated during the initial exploratory experimental studies (Table 2) indicates that a wide variety of such materials exists. Moreover, photo-induced pumping of ions through membranes is prevalent in nature and has been essential for the development of life. It is well known that photosynthetic electron transfer from the inside to the outside of the energy converting membrane is coupled with proton transfer in the opposite direction which builds up a proton gradient for the synthesis of adenosine triphosphate. The essential coupling element is a pool of plastoquinone molecules which is organized in such a way that it receives photoexcited electrons near the outer surface of the photosynthetic membrane and passes them on to plastocyanine near the inner surface. Simultaneously, protons are intercalated from the outside, transferred with the electrons to the inside and then deintercalated. Another example is found in the purple membranes of halobacteria [64] (Fig. 17). Bacteriorhodopsin, a protein similar to the visual pigment, forms patches with a hexagonal lattice. As a consequence of light absorption by its chromophore retinal, structural changes occur which mediate the uptake, transport and
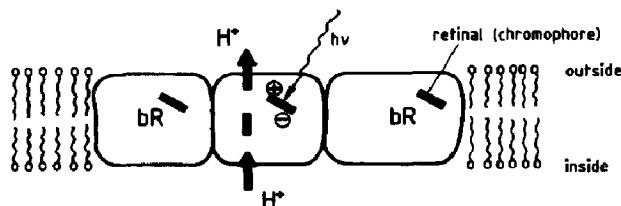
Fig. 17. Photo-induced proton pumping in the purple membranes of halobacteria.

release of protons (at the opposite side of the membrane). Although in this case excitation energy is not being transferred by electron conduction but energetically by structural changes, we are confronted with a photo-induced intercalation–deintercalation mechanism.

The fact that photo-induced ion transfer takes place in natural energy conversion systems suggests that it has potential for technical development. The simplest solar energy conversion systems based on this principle are shown in Fig. 18. One is a solar-powered ion pump consisting of a thin membrane which is placed in contact with two different electrolytes (in order to create an asymmetric system). Illumination of this membrane (which can also be asymmetric) results in a vectorial transfer of ions. The other system shown is a solar rechargeable intercalation battery consisting, for example, of a photosensitive cathode and a metallic conducting anode (a p–n arrangement with a photosensitive anode is also possible). During illumination cations (A^+) are photo-inserted into the cathode and the battery is charged. Discharge takes place in the dark.

Photo-induced proton transfer has been observed in perovskite-type $TiO_2(B)$ [49] which is stable in contact with water. Such systems are attrac-
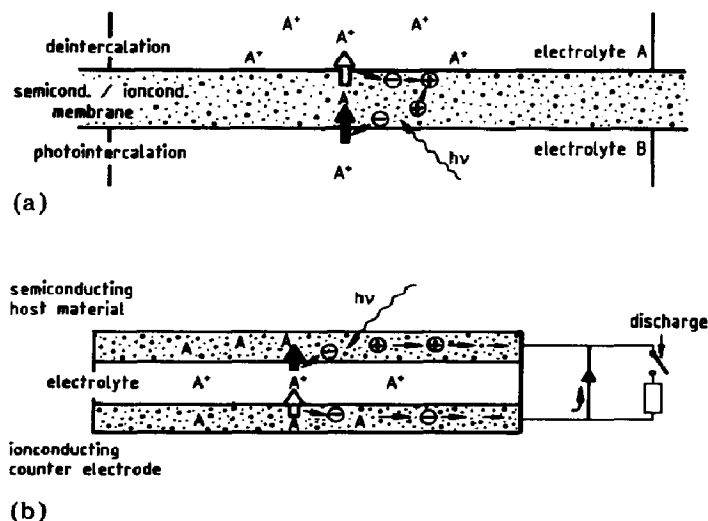

(a)

(b)

Fig. 18. Possible technological applications of photo-intercalation mechanisms: (a) photon-powered ion pumps; (b) photo-intercalation batteries.

tive, first because of the analogy with natural systems and secondly because of the comparably high mobility of protons in solids.

p-type $Cu_{6-x}PS_5I$ has been found to be an interesting host material for photo-intercalation (Fig. 19) [51]. The deintercalated material is opaque owing to the presence of colour centres (shaded area in the forbidden energy region). When Cu^+ is photo-intercalated the colour centres are neutralized and the compound becomes transparent to red light.

It can be seen that the result of the photo-induced strong surface interaction and ion transfer is optical information and energy storage. Many materials, particularly polymers, are in principle candidates for this type of mechanism.
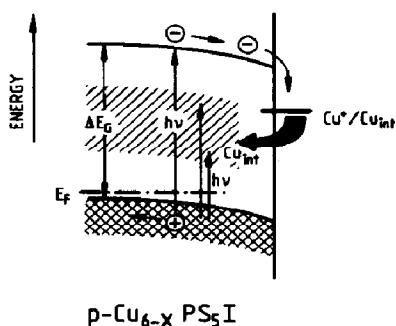

$p-Cu_{6-x}PS_5I$

Fig. 19. Energy scheme for the photo-intercalation of Cu^+ into $Cu_{6-x}PS_5I$.

7. Discussion

The experimental results presented here show that photoelectrodes which undergo a strong reversible interaction with reactants in the electrolyte offer new research and development possibilities for photoelectrochemical solar energy conversion and storage. Semiconductors with valence bands derived from transition metal d states facilitate many-electron transfer reactions utilizing low energy photons for the generation of solar fuels. All d band semiconductors investigated so far undergo photoreactions with water. Comparison of the series of compounds RuS_2, $RuSe_2$ and $RuTe_2$ has emphasized that the top of the valence band should be composed of relatively pure d states to facilitate the photo-induced liberation of oxygen from water. We believe that our proposal that photoelectrocatalysis can be improved by using pairs or clusters of transition metal atoms [39] is valid. However, we have not yet obtained experimental confirmation of this hypothesis. RuP_3 (ruthenium pairs) and ReS_2 (Re_4 clusters) photoreact with water but undergo degradation. We attribute this to an unfavourable easily oxidizable ligand (phosphorus) and tentatively to extremely strong O—Re bonds which prevent the surface-bound oxygen from reacting further to form molecular oxygen. It is obvious that the situation is more complicated than

was originally assumed. However, progress appears to be possible by performing straightforward experimental research.

Photo-induced ion transfer (photo-intercalation or deintercalation) is still in the early stages of experimental research. Many new materials with combined electronic–ionic conduction require investigation (Table 2). In this case strong photo-induced interfacial interactions lead to reversible solid state changes of the electrode material with the prospect of several useful applications (solar energy storage, information storage and photographic processes).

A common feature of photoelectrochemical reactions involving strong reversible surface interactions is that they cannot be described adequately using existing theoretical concepts. The strong bonding of redox species to semiconductor interfaces has a marked effect on the distribution of electron levels. The resulting high concentration of surface states shifts a significant fraction of the potential drop of the semiconductor surface into the Helmholtz layer. For ions photo-intercalated into semiconducting host materials the complications are even more significant. The electronic energy scheme, which is widely used for visualizing photoelectrochemical mechanisms, ceases to be strictly valid because the electrochemical potential of the intercalated ions contributes to the free energy of the electrodes. Therefore the energy bands may shift as a consequence of intercalation. In addition, the space charge layer may contract or expand owing to the introduction of ionic charge carriers.

Semiconductor–electrolyte interfaces which undergo strong reversible photo-induced interactions with redox species can be considered as dynamic systems. The energy bands of a d band semiconductor may shift until oxidation or reduction becomes possible (Figs. 11 and 12). In principle, it is no longer necessary to select semiconductors carefully according to their energy band position. The energy bands can be adjusted to the redox system. In principle, the systematic dependence of the photocurrent density curves for various redox systems on the electrode potential enables a kind of photopolarography to be performed. The redox system in the electrolyte can be identified by the electrode potential at which the photocurrents are produced. Measurement using lock-in techniques makes this analytical technique sensitive.

Our results may encourage researchers not to concentrate on photosensitive materials developed for semiconductor devices but to tailor new photoelectrodes for solar energy conversion and storage on the basis of electrocatalytic requirements. A large number of semiconducting compounds have not yet been investigated. The work with semiconducting cluster compounds, which we consider to be highly promising for the generation of solar fuel, and with photosensitive ion conductors may eventually become routine. In this case the semiconductor–electrolyte interface will cease to be a relatively sharp line between the solid state and electrochemical mechanisms and there will be a transition region where chemistry and the dynamics of chemical mechanisms will play a significant role in a loose permeable

skeleton composed of a crystalline or polymeric structure which will supply the photon-powered energy drive.

Acknowledgments

References

1 A. Fujishima and K. Honda, *Nature (London), 238* (1972) 37.
2 J. G. Mavroides, J. A. Kafalas and D. F. Kolesar, *Appl. Phys. Lett., 28* (1971) 241.
3 M. S. Wrighton, A. B. Ellis, P. T. Wolczanski, D. L. Morse, H. B. Abrahamson and D. S. Ginley, *J. Am. Chem. Soc., 98* (1976) 2774.
4 H. S. Jarret, A. W. Sleight, H. H. Kung and H. L. Gilson, *J. Appl. Phys., 51* (1981) 3916.
5 H. P. Maruska and A. K. Ghosh, *Sol. Energy, 20* (1978) 443; *J. Electrochem. Soc., 124* (1977) 1516.
6 G. Campet, M. P. Dare-Edwards, A. Hamnet and J. B. Goodenough, *Nouv. J. Chim., 4* (1980) 501.
7 P. Salvador, C. Gutierrez and J. B. Goodenough, *J. Appl. Phys., 53* (1982) 7003.
8 A. Heller and R. G. Vadimsky, *Phys. Rev. Lett., 46* (1981) 1153.
9 M. Noda, *Int. J. Hydrogen Energy, 7* (1982) 311.
10 L. A. Harris, M. E. Gerstner and R. H. Wilson, *J. Electrochem. Soc., 124* (1977) 1511.
11 F.-R. F. Fan, G. A. Hope and A. J. Bard, *J. Electrochem. Soc., 129* (1982) 1647.
12 G. A. Hope, F. R.-F. Fan and A. J. Bard, *J. Electrochem. Soc., 130* (1983) 1488.
13 H. Gerischer, Solar photoelectrolysis with semiconductor electrodes. In B. D. Seraphin (ed.), *Solar Energy Conversion, Top. Appl. Phys.,* (1979) 115.
14 M. F. Weber and M. J. Dignam, *J. Electrochem. Soc., 131* (1984) 1258.
15 H. Gerischer, *Proc. Workshop on Electrocatalysis on Non-Metallic Surfaces, Gaithersburg, MD, 1975, NBS Publ. 455,* 1976, p. 1 (National Bureau of Standards, U.S. Department of Commerce).
16 W. J. Plieth and K. J. Vetter, *Z. Phys. Chem. (Frankfurt am Main), 61* (1968) 282.
17 H. Tributsch, *Z. Naturforsch., 32a* (1977) 972.
18 H. Tributsch and J. C. Bennett, *J. Electroanal. Chem., 81* (1977) 97.
19 H. Tributsch, *Ber. Bunsenges. Phys. Chem., 81* (1971) 361.
20 H. Tributsch, *J. Electrochem. Soc., 125* (1978) 1086; *Ber. Bunsenges. Phys. Chem., 82* (1978) 169.
21 J. Gobrecht, H. Gerischer and H. Tributsch, *J. Electrochem. Soc., 125* (1978) 2085; *Ber. Bunsenges. Phys. Chem., 82* (1978) 1331.
22 H. Tributsch, *Sol. Energy Mater., 1* (1979) 705.
23 H. Tributsch, *Struct. Bonding (Berlin), 49* (1982) 127.
24 G. Kline, K. Kam, D. Canfield and B. A. Parkinson, *Sol. Energy Mater., 4* (1981) 301.
25 L. F. Schneemeyer and M. S. Wrighton, *J. Am. Chem. Soc., 101* (1979) 6496.
26 F. R.-F. Fan, H. S. White, B. Wheeler and A. J. Bard, *J. Electrochem. Soc., 127* (1980) 519.
27 H. J. Lewerenz, A. Heller and F. J. Di Salvo, *J. Am. Chem. Soc., 102* (6) (1980) 1877.

28 G. Kline, K. Kam, R. Ziegler and B. A. Parkinson, *Sol. Energy Mater.*, *6* (1982) 337.
29 H. Tributsch and U. Gorochov, *Electrochim. Acta*, *27* (1982) 215.
30 H. Ezzaouia, R. Heindl, R. Parsons and H. Tributsch, *J. Electroanal. Chem.*, *145* (1983) 279; *165* (1984) 155.
31 H.-M. Kühne and H. Tributsch, *J. Electrochem. Soc.*, *130* (1983) 1448.
32 H.-M. Kühne and H. Tributsch, *Ber. Bunsenges. Phys. Chem.*, *88* (1984) 10.
33 H.-M. Kühne and H. Tributsch, *J. Electroanal. Chem.*, in the press.
34 W. Jaegermann and H. Tributsch, *J. Appl. Electrochem.*, *13* (1983) 743.
35 A. Ennaoui and H. Tributsch, *Sol. Cells*, *13* (1984) 197; A. Ennaoui, S. Fiechter, W. Jaegermann and H. Tributsch, submitted to *J. Electrochem. Soc.*
36 A. Ennaoui, S. Fiechter, H. Goslowsky and H. Tributsch, *J. Electrochem. Soc.*, in the press.
37 H. Tributsch, to be published.
38 H. Tributsch and W. Hönle, *J. Electroanal. Chem.*, in the press.
39 H. Tributsch, in J. O'M. Bockris (ed.), *Modern Aspects of Electrochemistry*, Butterworths, London, in the press.
40 T. Hahn (ed.), *International Tables for Crystallography*, Reidel, Dordrecht, 1983.
41 H. Tributsch, *J. Electrochem. Soc.*, *128* (1981) 1261.
42 H. Tributsch, *Appl. Phys.*, *23* (1980) 61.
43 H. Tributsch, *Faraday Discuss. Chem. Soc.*, *70* (1980).
44 H. Tributsch, *Solid State Ionics*, *9 - 10* (1983) 41.
45 M. Abramovich, O. Gorochov and H. Tributsch, *J. Electroanal. Chem.*, *153* (1983) 115.
46 O. Gorochov, D. Schleich and H. Tributsch, to be published.
47 D. Schleich, H.-M. Kühne and H. Tributsch, to be published.
48 C. Levy-Clement and B. Theys, *J. Electrochem. Soc.*, *131* (1984) 1300.
49 G. Betz, H. Tributsch and R. Marchand, *J. Appl. Electrochem.*, *14* (1984) 315.
50 G. Betz, H. Tributsch and R. Brec, to be published.
51 G. Betz, H. Tributsch and S. Fiechter, *J. Electrochem. Soc.*, *131* (1984) 640.
52 G. Betz, M. Künst, J. G. Rabé and H. Tributsch, to be published.
53 H.-M. Kühne, *Ph.D. Thesis*, Free University of Berlin, 1985.
54 J. Horkans and M. W. Shafer, cited in J. W. Schultze, *Chem.-Ing.-Tech.*, *52* (1980) 447.
55 H.-M. Kühne, W. Jaegermann and H. Tributsch, *Chem. Phys. Lett.*, *112* (1984) 160.
56 F. A. Cotton and F. R. Walton, *Multiple Bonds between Metal Atoms*, Wiley, New York, 1982.
57 Ø. Fischer and M. B. Maple, in Ø. Fischer and M. B. Maple (eds.), *Top. Curr. Phys.*, *32* (1982).
58 A. Simon, *Naturwissenschaften*, *71* (1984) 171.
59 H. Imoto and A. Simon, *Inorg. Chem.*, *21* (1982) 308.
60 D. Schmeisser, personal communication, 1984.
61 A. Perrin, M. Sergent and Ø. Fischer, *Mater. Res. Bull.*, *13* (1978) 259.
62 A. Perrin, R. Chevrel, M. Sergent and Ø. Fischer, *J. Solid State Chem.*, *33* (1980) 43.
63 W. Hönle and K. Yvon, *Z. Kristallogr.*, *162* (1983) 703.
64 W. Stockenius, *Acc. Chem. Res.*, *13* (1980) 337.